lubricants

Article

Influence of Nozzle Layouts on the Heat-Flow Coupled Characteristics for Oil-Jet Lubricated Spur Gears

Duan Yang [1,2], He Liu [1], Jianfeng Zhong [1,2], Xiang Zhu [1] and Yu Dai [1,*]

[1] College of Mechanical and Electrical Engineering, Central South University, Changsha 410083, China
[2] Hunan Aviation Powerplant Research Institute, AECC, Zhuzhou 412002, China
* Correspondence: 210143@csu.edu.cn

Abstract: Aiming to explore the influence of nozzle layouts on the lubrication and cooling performance of spur gears under oil jet lubrication conditions, this paper introduces a heat-flow coupled analysis method to predict the temperature field of the tooth surface with different nozzle layouts. Firstly, the friction heat formulas integrating the coefficient of friction and average contact stress are presented for calculating heat generation. We also present the impingement depth model, which considers the nozzle orientation parameters, jet velocity, and gear structure of the given spur gear pair for laying out the nozzle. Then, a heat-flow coupled finite element analysis method is exploited to resemble the jet lubrication process and gain the gear temperature characteristics. Finally, the numerical results of this model compare well with those of the experiments, showing that this heat-flow coupled model provides accurate temperature prediction, indicating that the nozzle layouts determined as a function of the oil jet height, deviation distance, and oil injection angle significantly influence the lubrication and cooling performance. Further, this study also reveals that the lubrication performance in cases where the nozzle approaches the side of the pinion is relatively superior.

Keywords: spur gear pairs; jet lubrication; nozzle layout; heat-flow coupled analysis

check for updates

Citation: Yang, D.; Liu, H.; Zhong, J.; Zhu, X.; Dai, Y. Influence of Nozzle Layouts on the Heat-Flow Coupled Characteristics for Oil-Jet Lubricated Spur Gears. *Lubricants* **2023**, *11*, 25. https://doi.org/10.3390/lubricants11010025

Received: 16 November 2022
Revised: 6 January 2023
Accepted: 7 January 2023
Published: 8 January 2023

1. Introduction

Service life and efficiency are critical requirements for the gearing system in the aeronautic and automobile industries. Spur gears are the most common and important reduction gears in an aero-engines' main reducer. Suffering from complex working conditions, high-speed and heavy-duty spur gears always generate huge mechanical power losses; these losses are converted into considerable amounts of heat and cause an excessive temperature rise. As known to all, excessive temperatures are more likely to lead to scuffing failure [1,2]. Generally speaking, oil jet lubrication is a practical and effective method to reduce the failure risk and prolong the viability of the gearing system [3–6]. Based on the heat-flow coupled analysis method, a better nozzle layout is the prerequisite to achieving better lubrication performance, as evaluated by the temperature distribution characteristics.

The development of gear elastohydrodynamic lubrication models to investigate the tribology process on the tooth surface has recently become mainstream. Normally, the models incorporate the Reynolds equation for determining the pressure distribution and the elastic deformation equation based on the elastic half-space theory. Dowson and Higginson [7] first investigated the line of isothermal elastohydrodynamic contacts. Incorporating different rheological behaviors, Yang and Wen [8] expanded the generalized Reynolds equation that concerned non-Newtonian fluid performance and the thermal effect on fluid properties and used it for studying the effect on film and pressure distributions. However, the studies mentioned above ignored the action of the gear surface's roughness; the results given in [9,10] considered surface asperities, and the asperities were replaced with the specified statistical models. Likewise, a model was developed for processing the gear contacts under mixed friction conditions [11]. By incorporating the two-dimensional roughness of the contact surfaces based on real-measured data and leveraging an empirical load-sharing formula, this model could calculate the pressure distributions of the spur gears. Apart from two-dimensional contacts, various numerical solutions are more concerned with three dimensions for ascertaining the impact of tooth width, including crowning, chamfering, and filleting; some relevant studies [12–14] reagrding line contacts are available. By leveraging the multigrid method, Venner [15] accelerated the convergence process of the elastohydrodynamic contacts.

In terms of temperature distributions on the tooth surface, heat transfer is the prerequisite for a dependable analysis. Convective heat exchange occurs between lubricating oil, surrounding air, and solid gears. Considerable amounts of frictional heat are transferred by lubricating oil to push the gear to achieve a heat balance with the surroundings in the event of an excessive temperature, and thus heat convection of the meshing area is also closely related to lubricating oil [16–18]. Previous thermal elastohydrodynamic lubrication studies were limited to the distribution of temperature gradients in local contact areas. Nevertheless, the finite element method is a more efficient means of dealing with various heat exchanges. To explore these and more, earlier studies focused on the bulk and transient temperature fields for spur gears [19], for spiral bevel gears [20]. Following that, subsequent research continued to investigate temperature distributions of a variety of gears [21–23]. Meanwhile, the heat flux, heat exchange, gear geometry parameters, etc., have been considered. More than that, Zhang et al. [24] predicted the bulk temperature assuming that the heat flux in a period of rotation is continuous with the aid of the EHL method.

Lubrication performance is strongly affected by the nozzle layouts under oil jet lubrication; therefore, a novel gear impingement depth mathematical model has been introduced to determine the oil nozzle layouts [25–27]. The rapid development of computational fluid dynamics (CFD) technology has allowed for its used as an effective tool for the deep understanding of real practical engineering problems [28–30]. Subsequently, to verify the mathematical model, a computational fluid dynamics model was established and applied to simulate the injection process with the aim of assessing the lubrication performance [31]. The results showed that the oil-air ratio and total pressure in the meshing region are significantly positively related to the impingement depth. Other researchers [5,6] have come up with similar results validating through experiments that the nozzle location affects the oil-air ratio and total pressure. On this basis, the complex impingement depth model is extended for the face gear and spiral bevel gear [32–34]. However, the aforementioned literature determined the nozzle layouts judged by the oil-air ratio and total pressure which are hard to measure directly through an indirect method.

The following paper presents an alternative numerical method combining the gear elastohydrodynamic lubrication method with the heat-flow coupled FEM to resemble the rotation of the spur gears under jet lubrication. Firstly, the generated frictional heat is captured by calculating the friction coefficient with the EHL model and then determining the contact stress and sliding velocity through a tooth surface contact analysis. Meanwhile, an impingement depth model for spur gear is also given; it integrates oil jet height, deviation distance, oil injection angle, and gear parameters. Finally, by leveraging the FEM analysis, the heat-flow coupling analysis method is developed to predict the temperature distribution characteristics of spur gears under different nozzle layouts, and the numerical results are compared with the corresponding impingement depths and experimental findings.

2. Analytical Model

2.1. Kinematics Analysis

By definition, the pinion and gear share an arbitrary contact point, which is the common tangent of the base circles (see Figure 1). The meshing process is from point A to point B, where A (B) denotes the cross point of the outside circle of the gear (pinion) with the contact path. The parameter s_{y0} is introduced to define the meshing location from point A (Figure 1).

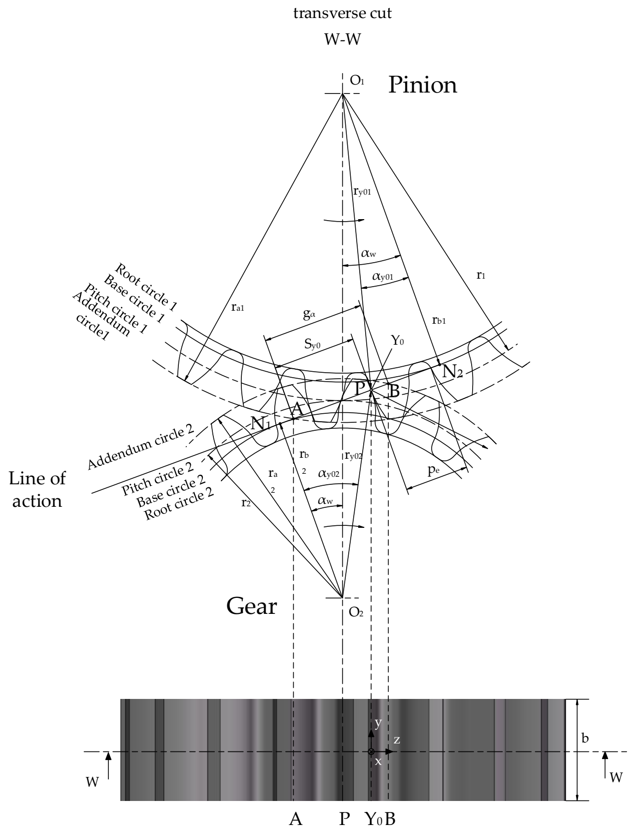

Figure 1. The meshing of a gear pair.

The kinematic parameters of meshing points for the involute gears can be expressed as:

$$\begin{cases} s_P = \sqrt{(d_{a1}^2 - d_{b1}^2)/4} - \frac{d_1 \sin\alpha}{2} \\ s_B - s_P = \sqrt{(d_{a2}^2 - d_{b2}^2)/4} - \frac{d_2 \sin\alpha}{2} \\ R_1 = \frac{1}{2} d_1 \sin\alpha + (s_P - s) \\ R_2 = \frac{1}{2} d_2 \sin\alpha - (s_P - s) \\ R = \frac{R_1 R_2}{R_1 + R_2} \\ u_{1,2} = \omega_{1,2} \times R_{1,2} \\ u_s = u_1 - u_2 \\ u_e = (u_1 + u_2)/2 \\ \delta = u_s/u_e = 2(u_1 - u_2)/(u_1 + u_2) \end{cases} \tag{1}$$

where d_{a1} and d_{a2}, respectively, denote the outside diameter of the pinion and gear, d_{b1} and d_{b2}, respectively, denote the base diameter of the pinion and gear, d_1 and d_2, respectively, denote the pitch diameter of the pinion and gear, and α represents the pressure angle. R_1 and R_2, respectively, denote the curvature radius of the pinion and gear, and R is the synthetic curvature radius. u_1 and u_2, respectively, denote the speed of the pinion and gear at the arbitrary contact point, and ω_1 and ω_2, respectively, denote the angular speed of the pinion and gear at the arbitrary contact point. u_s and u_e, respectively, denote the relative sliding velocity and entrainment velocity, and δ denotes the slide–rolling ratio at an arbitrary meshing point. The subscripts A, B, and P represent the location of the contact point on the contact path.

The normal load F_n and maximum equivalent Hertzian contact stress σ_H at the contact point can be calculated as follows:

$$\begin{cases} F_n = \frac{Kz_1T_2}{r_c z_2 L\cos\alpha} \\ \sigma_H = \left(\frac{F_n E}{2\pi R}\right)^{0.5} \\ b = \sqrt{\frac{8F_n R}{\pi E}} \end{cases} \tag{2}$$

where K denotes the load-distributing factor between teeth. E $\left(2/E = \left[\left(1-\nu_1^2\right)/E_1 + \left(1-\nu_2^2\right)/E_2\right]\right)$ represents the equivalent elastic modulus. L is the active contact length and b is the half-width of Hertzian contact.

2.2. Elastohydrodynamics

Given that there is no great change in temperature under the light load and low-speed conditions in this paper, the thermal effect of lubricating oil is not considered. For EHL lubrication conditions, the following basic equations need to be solved:

Reynolds equation:

$$\frac{d}{dx}\left(\frac{\rho h^3}{\eta}\frac{dp}{dx}\right) = 12u_e\frac{d(\rho h)}{dx} + 12\rho\frac{\partial h}{\partial t} \tag{3}$$

where p denotes the oil film pressure, ρ and η are the oil density and viscosity, respectively.

Considering the gear profile and surface roughness, the film thickness equation is as follows:

$$h(x) = h_0 + \frac{x^2}{2R} + \delta_{y1}(x) + \delta_{y2}(x) + v(x) \tag{4}$$

where h_0 denotes central oil film thickness. $\Delta_{y1}(x)$ and $\delta_{y2}(x)$ represent the roughness height. Weierstrass-Mandelbort function (i.e., W-M function) is adopted to simulate the variety of the roughness [10]. V (x) is the elastic deformation and can be determined by

$$v(x) = -\frac{2}{\pi E}\int_{s_0}^{s_e} p(s)\ln(s-x)^2 ds \tag{5}$$

The oil viscosity and density equations which are assumed to be functions of pressure are respectively expressed as:

$$\eta = \eta_0 \exp\left\{(\ln\eta_0 + 9.67)\left[\left(1+\frac{p}{p_0}\right)^z - 1\right]\right\} \tag{6}$$

and

$$\rho = \rho_0\left[1 + \frac{0.6\times 10^{-9}p}{1+1.7\times 10^{-9}p}\right] \tag{7}$$

where η_0 is viscosity (at p = 0, T = 30 °C). p_0 is the pressure coeffcient (in this paper, $p_0 = 1.96 \times 10^8$). z is the pressure-viscosity coefficient (in this paper, z = 0.68).

Force equilibrium equation:

$$w = \int_{x_0}^{x_e} p(x)dx p(x) = \begin{cases} p_h & h > \varepsilon \\ P_a & h \le \varepsilon \end{cases} \tag{8}$$

where w is the normal load applied per unit length. p_h and p_a, respectively, denote the hydrodynamic pressure and the asperity pressure. ε denotes the local critical oil film thickness; in this study ε = 10 nm. Readers are referred to the pertinent literature about the detailed calculation instructions for this mixed EHL lubrication [35].

2.3. Friction Coefficient and Heat Generation

The mixed friction heat is generated from the shear of hydrodynamic lubrication and asperity contact. Considering the non-Newton characteristics [36], the shear stress of hydrodynamic lubrication τ_h of a can be determined by:

$$\dot{\gamma} = \frac{\dot{\tau}}{G_\infty} - \frac{\tau_L}{\eta}\ln\left(1 - \frac{\tau_h}{\tau_L}\right) \tag{9}$$

where τ_L and G_∞, respectively, denote the limiting shear stress and shear elastic modulus. The boundary friction τ_a of asperity contact can be expressed as:

$$\tau_a(x) = f_c \times p_a(x) \tag{10}$$

where the asperity friction coefficient f_c is closely related to the roughness and simplified as a constant in the range of 0.07–0.15 [37,38]; in this study, f_c = 0.15. Hence, the friction F_f and the friction coefficient f_{mix} are commonly written as:

$$F_f = \int_{x_0}^{x_e} \tau(x)dx \; \tau = \begin{cases} \tau_h & h > \varepsilon \\ \tau_a & 0 < h \leqslant \varepsilon \end{cases} \tag{11}$$

and

$$f_{mix} = \frac{F_f}{w} \tag{12}$$

The friction power loss Q, which would convert to friction heat, can be expressed as:

$$Q = f_{\text{mix}} \times w \times u_s \tag{13}$$

Generally, the heat distributions on the pinion face and gear face are different. By introducing a heat distribution coefficient, β, the heat flux density, q_i is written as:

$$q_i = \beta \times f_{\text{mix}} \times P_i \times u_s \tag{14}$$

For the bulk temperature field analysis, the transient process of friction heat generation can be regarded as a steady process during a rotation period.

$$\begin{cases} q_{1avc} = \frac{bn_1}{30U_1} q_1 \\ q_{2avc} = \frac{bn_2}{30U_2} q_2 \end{cases} \tag{15}$$

2.4. Heat Exchange

Heat convection is a very serious message to predict the bulk and flash temperature behavior of the gear. Here, a single-tooth model is used to investigate the convection heat transfer process with lubricating oil and the surrounding air. The boundary conditions for the tooth, including the end face, meshing, and other faces are shown in Figure 2.

(1) The meshing face

In general, convectional heat flow between the meshing face and the surrounding fluid is forced convection; hence, the corresponding convective heat transfer coefficient h_m is calculated as [39]:

$$h_m = 0.228 {Re_m}^{0.731} {Pr_m}^{0.333} \frac{\lambda_m}{d} \tag{16}$$

where the Reynolds number $Re_m = \omega {r_l}^2 / v_{oil}$ and r_l represent the turning radius. The Prandtl number $P_r = \rho v_{oil} c_p / \lambda$ [40], and c_p are the specific heat capacities of the lubricant. λ_m is the thermal conductivity of the lubricant.

(2) The end faces

The end faces always convect with the surrounding air, therefore, the corresponding convective heat transfer coefficient h_e of the laminar flow is given as [21,38]:

$$h_e = 0.308\lambda_{\text{air}}(m+2)^{0.5}Pr_e^{0.5}\left(\frac{\omega}{\nu_{\text{air}}}\right)^{0.5} \tag{17}$$

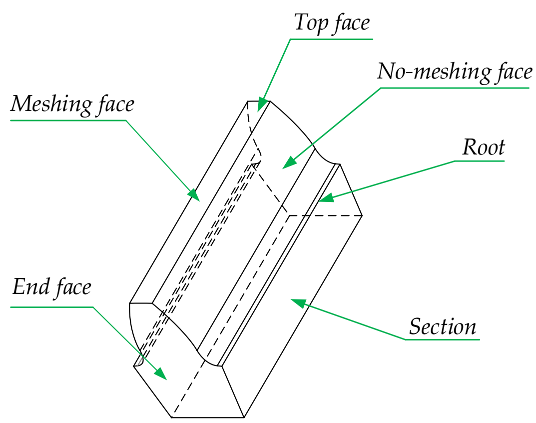

Figure 2. Boundary conditions of a single tooth model.

(3) Other faces

The convective heat transfer coefficients of other faces are assumed to be consistent [21,38]. To facilitate calculation, they are typically 1/3–1/2 h_e.

2.5. Temperature Prediction

The temperature behaviors of the tooth are individually simulated by leveraging ANSYS. The time-averaged heat flux $\overline{q}_{\text{i}}$ and boundary conditions of convection heat exchange in Section 2.4 are applied on the meshing face of the single tooth to predict the bulk temperature. As for transient temperature, the transient heat flux is continuously loaded on the single tooth by discretizing each meshing contact into N steps based on the average value of the steady temperature field as the initial, as shown in Figure 3.

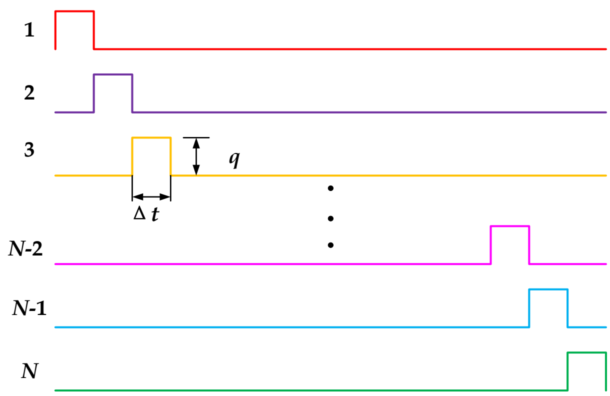

Figure 3. The transient heating process of a single gear.

3. Oil Jet Layout

3.1. Impingement Depth

In the aero-engine industry, determining the layout of oil jet nozzles for lubricating and cooling the gear pair is often deeply dependent on the engineer's experience and it is difficult to achieve an ideal lubrication performance. Akin et al. [24–26] are the pioneers that introduced the impingement depth d_p to study the performance of different lubrications (defined as shown in Figure 4a). A positive relationship between the impact depth and lubrication performance has been proved [41]. As illustrated in Figure 1a, the layout of the nozzle can be fixed by the oil jet height H, deviation distance L, offset distance S, and injection angle β.

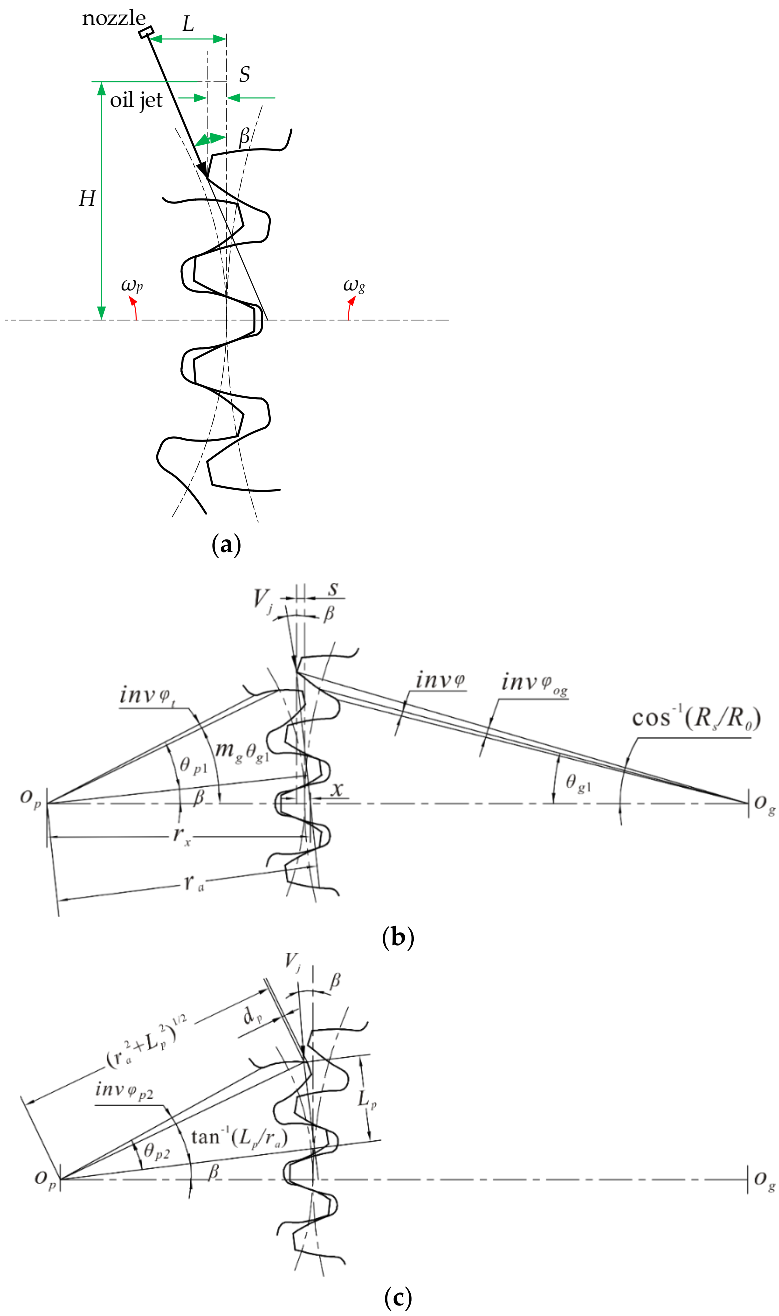

Figure 4. Diagram of pinion impingement depth: (**a**) Layout parameters of the nozzle; (**b**) Diagram of pinion impact depth (t_0 = 0); (**c**) Diagram of pinion impact depth (t_1 = t).

According to Wang et al. [41], the pinion impingement depth can be calculated by:

$$\begin{cases} d_p = \frac{z_1 m}{2} + m - \sqrt{\left((r - S + R_i \cdot \tan\beta) \cdot \cos\beta\right)^2 + L_p^2} \\ L_p = \frac{\left(R_o^2 - R_S^2\right)^{\frac{1}{2}}}{\cos\beta} - \frac{V_j(\theta_{p2} - \theta_{p1})}{w_p} - (r - S + R_i . \tan\beta) . \sin\beta \end{cases} \quad (18)$$

where the subscripts p represents the pinion. θ_{p1} is the initial angle (see Figure 4b); θ_{p2} is the angular position as the pinion is rotated t s (see Figure 4c); R_o, and R are the outside radius and pitch radius of the gear, respectively. R_i is the normal offset, and $R_s = R + S$.

3.2. Finite Element Model

At present, the generating heat cannot be added to the interface in ANSYS. In this study, the transient temperature distribution has three components: a transient temperature field module, a flow field module, and a heat-flow bidirectional coupling module (see Figure 5). The transient temperature field realizes the heat generation and conduction towards the gear body, and the flow field analysis is the oil jet lubrication realization process. The heat-flow coupling process is mainly used to transmit real-time data between the transient temperature and flow field.

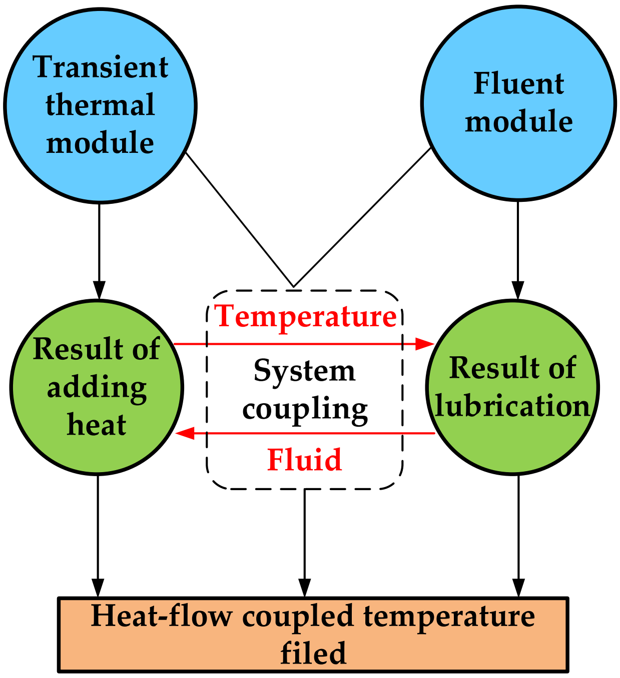

Figure 5. Diagram of the heat-flow coupling.

Following that, this paper presents in brief the appropriate models established for the transient temperature and flow field analysis:

(1) Temperature field

The temperature field module is a framework for simulating the heat generation of the tooth surface. Figure 6 shows the mesh model. The local mesh refinement approach for gear surfaces is used after the grid independence test is made; the element size is 1.2 mm. The average temperature obtained from the steady temperature analysis of a single gear tooth is regarded as the initial temperature condition. Similar to Figure 3, the heat of sliding friction is divided into consecutive steps and loaded on the surface according to the analysis in Section 2.

(2) Fluid field

The flow field module is mainly for simulating the oil stream sprayed from the nozzle to the gear surfaces. Similarly, based on the local mesh refinement and the grid independence test, the CFD mesh model is depicted in Figure 7, in which the global grid size is 0.006 m, the local grid size for gear surfaces, and the nozzle exit is 0.0006 m, and the grid quality exceeds 0.32.

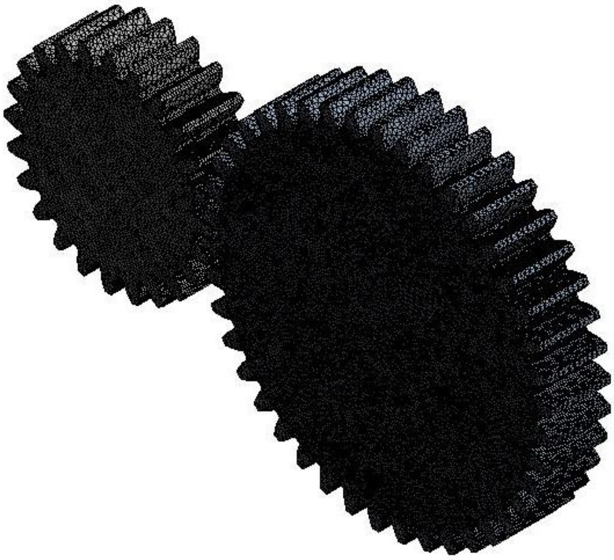

Figure 6. Mesh models in the temperature module.

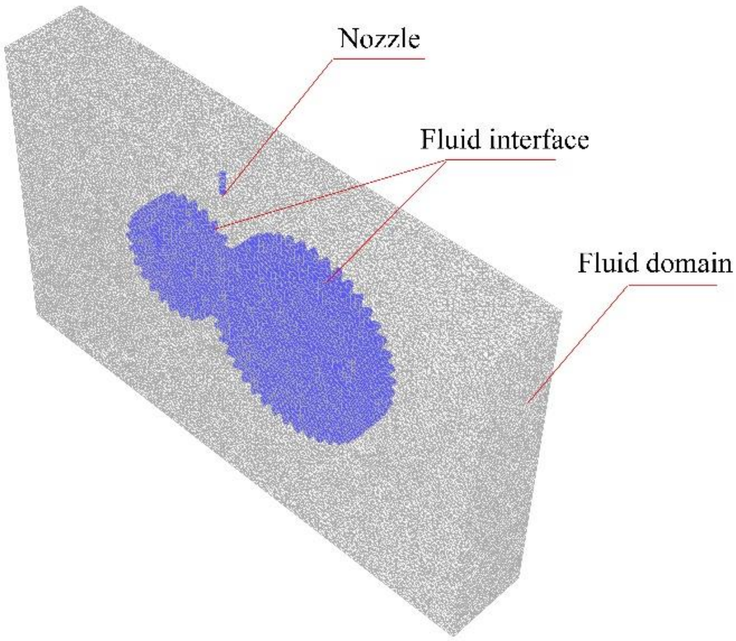

Figure 7. CFD Mesh models.

(3) Boundary conditions

The VOF (the main phase is air, the second phase is oil) and RNG turbulence methods are employed to address the oil-air two-phase flow. Energy equations are used, the y+ of all simulations is between 30 and 50, and standard wall functions are exploited for near-wall treatment. The material properties of the gear pair are the same as those listed in Section 2.1, and the main properties of lubricating oil and air are listed in Tables 1 and 2. The nozzle exit is set as the velocity inlet with a velocity of 5 m/s, the nozzle diameter is 2 mm, and the outside surfaces of the fluid domain in Figure 7 are set as the pressure outlet. The gear surfaces are regarded as the system coupling wall, and the dynamic mesh method in ANSYS Fluent is used for simulating the gear rotation. The time step of the transient temperature and flow field analysis is 1×10^{-5} s.

Table 1. Thermophysical parameters of lubricating oil.

Temperature (°C)	Thermal Conductivity Coefficient (W/m·°C)	Specific Heat (J/kg·°C)	Density (kg/m^3)	Kinematic Viscosity (mm^2/s)	Prandtl Number
50	0.152	1910	971.2	17.4	212.34
100	0.146	2070	970.4	5.00	68.79
158	0.139	2260	967.8	4.11	64.67

Table 2. Thermophysical parameters of air.

Temperature (°C)	Thermal Conductivity Coefficient (W/m·°C)	Specific Heat (J/kg·°C)	Density (kg/m^3)	Kinematic Viscosity (mm^2/s)	Prandtl Number
20	2.59	1005	1.208	15.06	0.703
40	2.76	1005	1.128	16.96	0.699
60	2.90	1009	1.060	18.97	0.696
80	3.05	1009	1.000	21.09	0.692

4. Results and Discussion

4.1. Numerical Results Analysis

The geometrical and working condition parameters of spur gears in this paper are listed in Table 3. Elasticity modulus and Poisson's ratio of the pinion and gear are $E_1 = E_2 = 210$ GPa and $v_1 = v_2 = 0.3$, respectively. The specific heat is 500 J/(kg·K), the heat conductivity coefficient is 40 W/(m·K), the density is 7800 kg/m^3, and the gear surface roughness is 0.6 µm.

Table 3. Geometrical and working condition parameters of spur gears.

Parameter	Value
Gear ratio z_1/z_2	24/42
Modulus m/(mm)	4
Tooth width B/(mm)	30
Rotation speed of pinion n_1/(r/min)	1500
Output torque T/(Nm)	200

The change in curvature radius and velocity along the contact path are presented in Figures 8 and 9, respectively. There is no gear modification for the involute spur gear pair. The change rules for load sharing and contact stress are shown in Figures 10 and 11, respectively.

The Reynolds equation, integrated with the film thickness equation, is used to estimate the Hertzian contact stress at the point of gear engagement on the area of tooth contact, which is the main source of heat generation. The dimension of the oil-filled gap is about 0.2~0.4 µm. The entrainment velocity at the meshing point is roughly equivalent to the slit wall motion velocities.

Finally, the distributions of average heat flux are depicted in Figure 12 through the above Equations (10)–(16). It indicates that the heat flux distributions are more susceptible to relative sliding velocity than the meshing force, in conjunction with Figures 9 and 10.

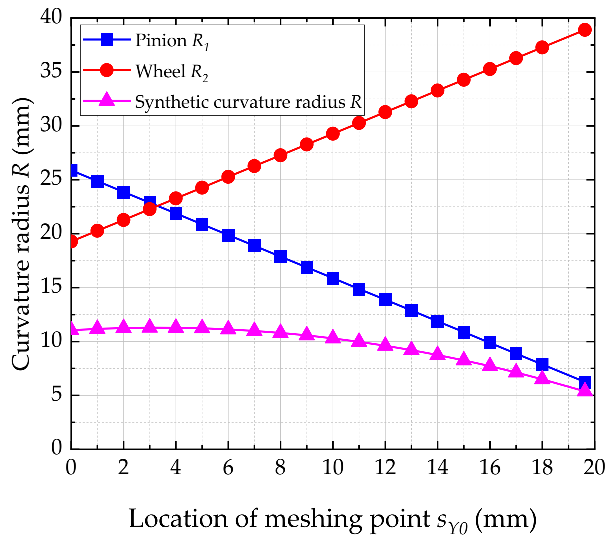

Figure 8. Curvature radius along the contact path.

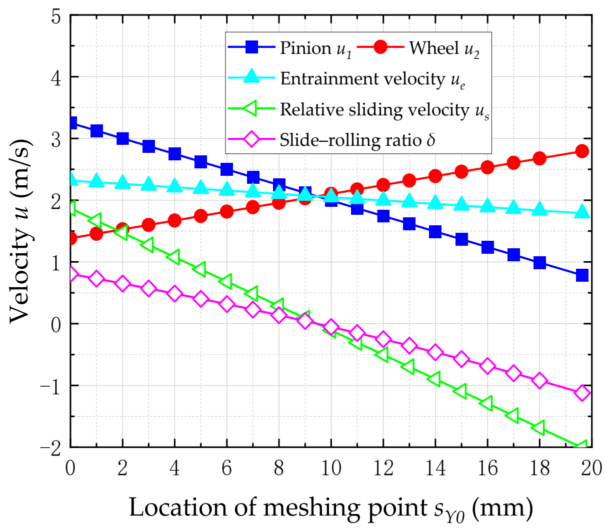

Figure 9. Velocity of the meshing point changes along the contact path.

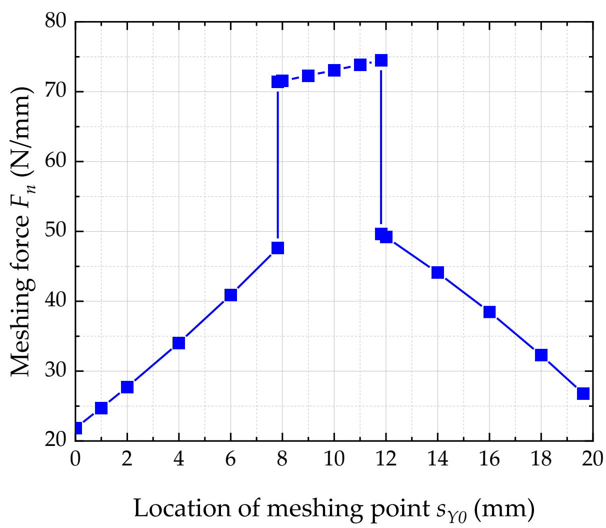

Figure 10. Meshing force versus contact path.

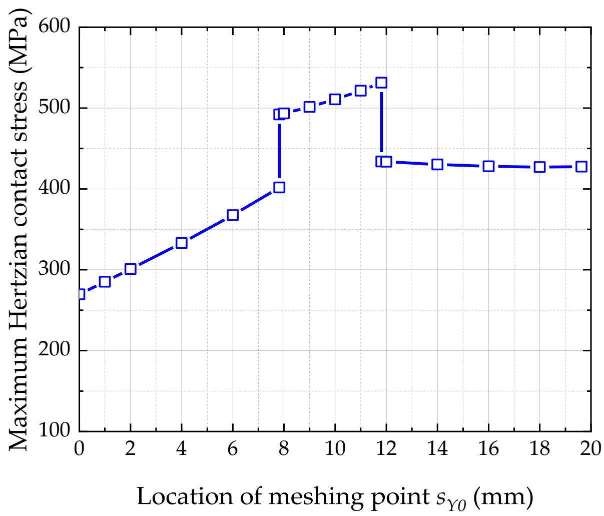

Figure 11. Maximum Hertzian contact stress versus the contact path.

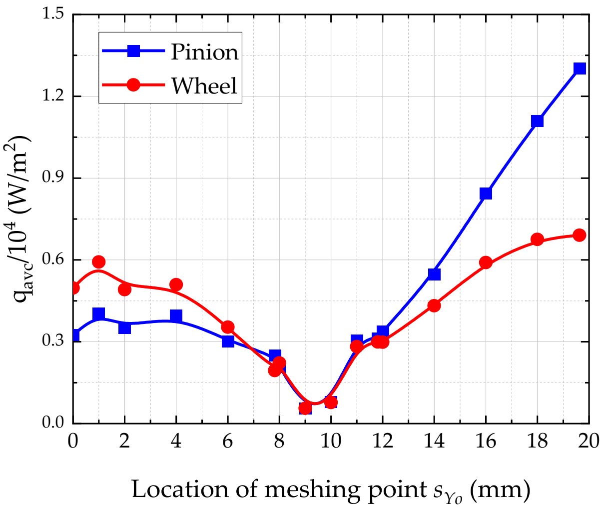

Figure 12. Distributions of average heat flux versus the line of action.

4.2. Bulk Temperature

According to Section 2.4 and Tables 1 and 2, the convective heat transfer coefficients of the meshing face and end face are confirmed as 3082.6 W/(m^2·°C), 626.6 W/(m^2·°C) for the pinion and 2651.8 W/(m^2·°C), 472.7 W/(m^2·°C) for the gear, respectively. Together with the average heat flux calculated in Section 2.3 (the main concern in this paper is the frictional heat generated by sliding friction between meshing gears (i.e., the tangent of the surface to the movement of the surface), while the rolling friction between meshing surfaces, the friction caused by gear deformation, and other heat generation caused by churning or windage behaviors on other faces can be ignored), the bulk temperature distribution characteristics on the single tooth are determined as shown in Figure 13. The temperature ranges from 75.3 °C to 77.3 °C for the pinion and from 72.3 °C to 74.8 °C for the gear. The high-temperature part is on the meshing face, close to the root for the pinion, and close to the addendum for the gear. Besides, the sub-high temperature area appears on the addendum for the pinion and on the root for the gear. This is because the maximum sliding velocity and heat flux occur in these regions. To be more specific, combining Figures 9 and 11, the largest relative sliding velocity occurs near the root and addendum of the gears, while the relative sliding velocity is approximately zero at the pitch radius. The maximum Hertzian contact stress is near the pitch radius. Hence, the largest heat generation occurs near the root of the pinion, the addendum of the gear. It is noticed that the convective heat transfer coefficients of the meshing face for the pinion are greater than those of the gear. These factors contribute to this temperature distribution. Additionally, the peak value on the pinion is higher than that on the gear; this suggests that the pinion temperature should be a major priority on the premise that the gear pair has the same materials.

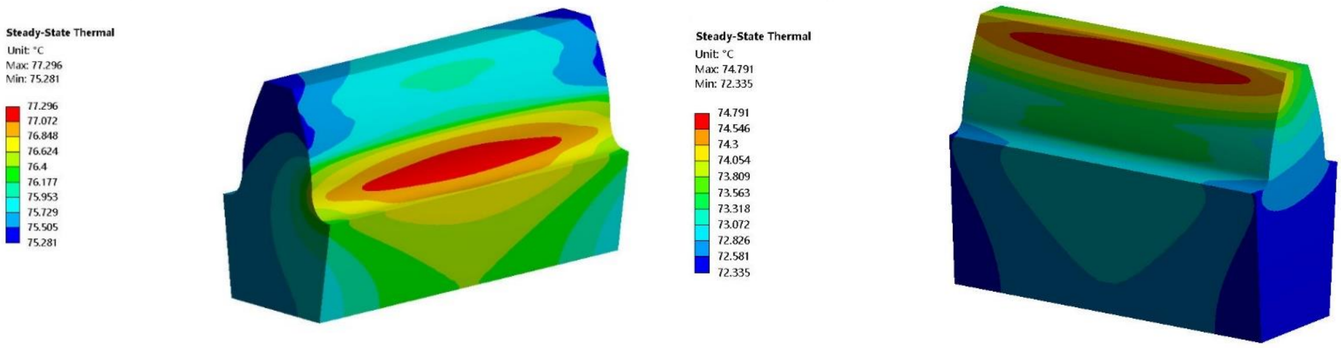

(**a**) (**b**)

Figure 13. Bulk temperature distribution of a single tooth: (**a**) pinion, (**b**) gear.

4.3. Transient Temperature

The impingement depth of the pinion and the gear of different layouts are determined according to the impingement depth in Section 3.1 and listed in Table 4. According to the nozzle parameters shown in Table 4 and the thermal analysis method in Section 3.2, the transient temperature distribution characteristics of the gear pair with different layouts under out-of-mesh conditions are obtained, as shown in Figure 13. The negative temperature values are due to the environmental temperature of zero degrees centigrade. When the nozzle is close to the pinion (see Figure 14a,b), the lubricating oil quantity in the meshing region is relatively large, and the tooth in the meshing zone experiences a low temperature, as shown in Figure 15a,b. As a result of more lubricating oil entering the meshing region, the tooth surface is well-lubricated and cooled. As can be seen in Figure 15b, light colors of the tooth surface in the meshing region are the most widely distributed, and the temperature is comparatively low. Meanwhile, when the nozzle is close to the pinion with a small oil injection angle as listed in Table 4 (see Figure 15b), the extreme on the tooth surface is lower than others, indicating that in this nozzle configuration, the lubrication and cooling performance is best.

Table 4. Theoretical values of impingement depth.

Group	Oil Jet Height H (mm)	Deviation Distance L (mm)	Oil Injection Angle β (°)	Impingement Depth of Pinion (mm)	Impingement Depth of Gear (mm)
1	100	1.2	0	0.92198	0.29226
2	100	8.2	5	1.1768	0
3	100	0	0	0	1.2836

4.4. Verification of Models

Aiming to validate the applicability and feasibility of the impact depth model and the numerical analysis method for predicting the transient gear temperature field under oil jet lubrication, our group [32] has performed the corresponding experiments as shown in Table 4, and the main gear geometry parameters are listed in Table 1. The specific test bench (see Figure 16), mainly comprises a spur gearbox connected with the driving and loading motors and equipped with a nozzle adjustment device.

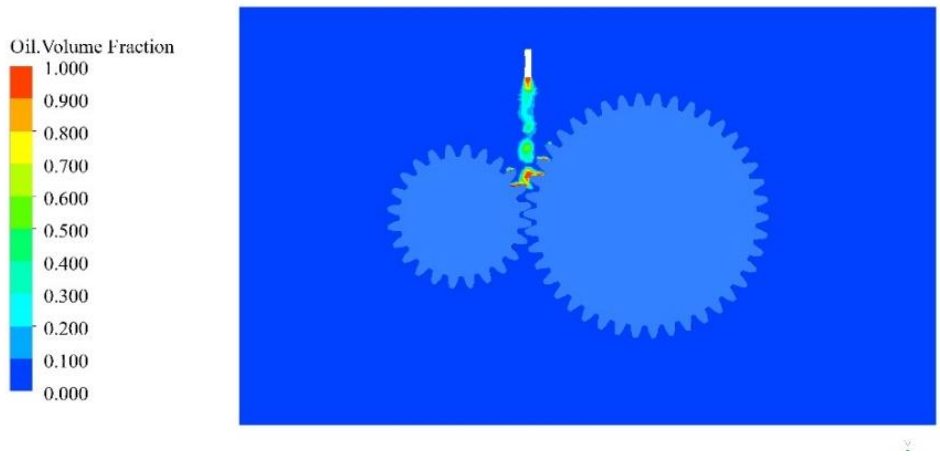

(**a**)

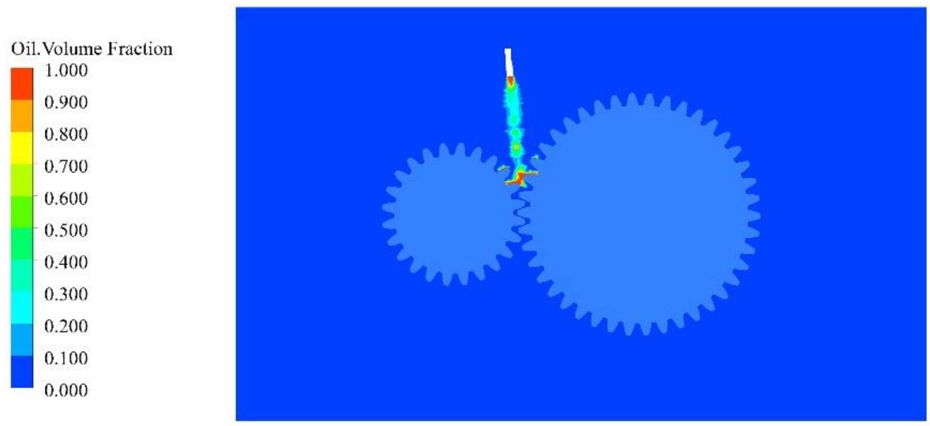

(**b**)

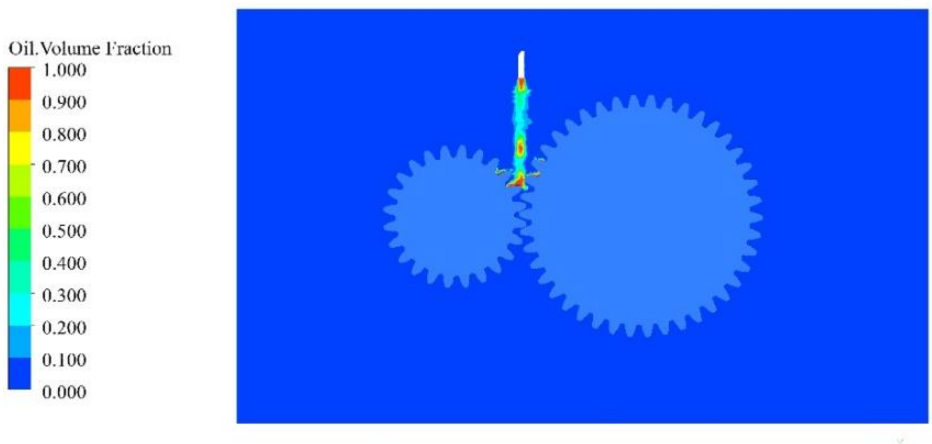

(**c**)

Figure 14. Oil volume fraction distribution characteristics of the gear pair versus different nozzle parameters: (**a**) Group 1; (**b**) Group 2; (**c**) Group 3.

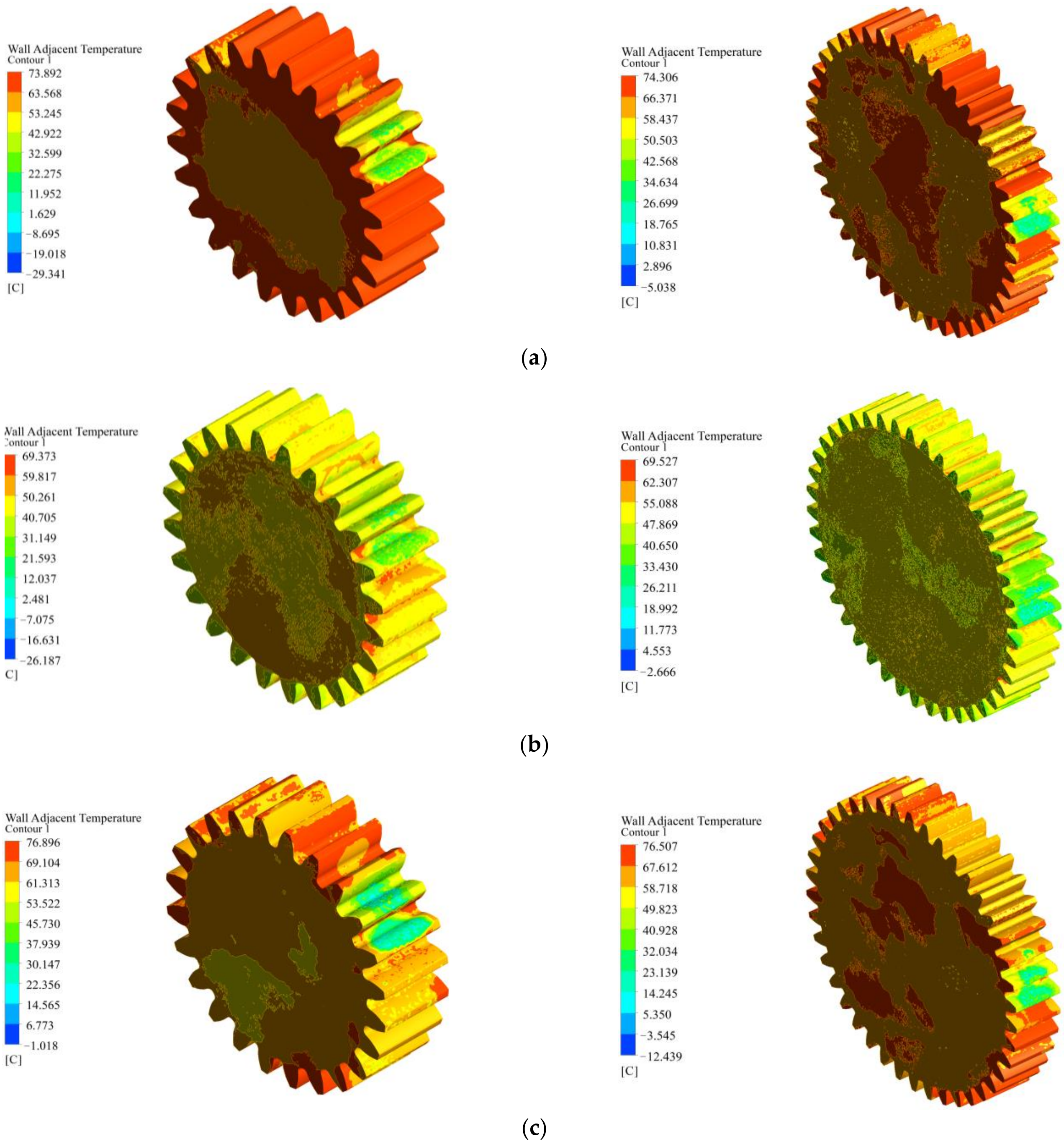

Figure 15. Temperature field characteristics of the pinion against different nozzle parameters: (**a**) Group 1; (**b**) Group 2; (**c**) Group 3.

Figure 17 illustrates the lubricating oil injection phenomenon with a high-speed camera. Besides, the tooth surface temperature was captured via a thermal infrared imager, as shown in Table 4. The captured infrared thermography for Group 2 in Table 4 is depicted in Figure 18.

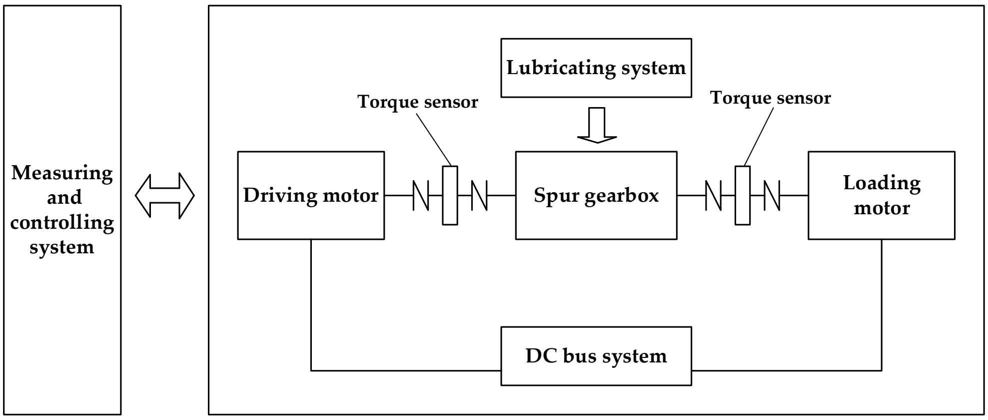

(**a**)

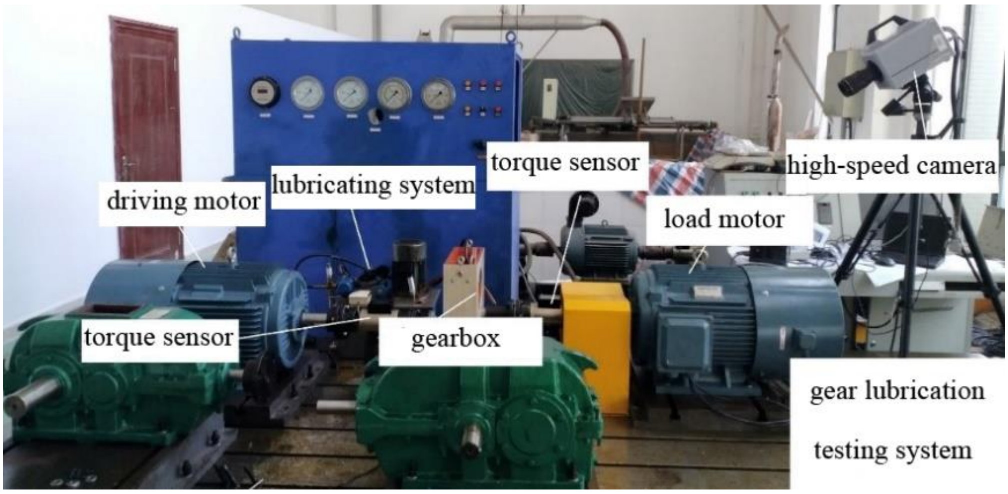

(**b**)

Figure 16. Specific test bench: (**a**) schematic diagram; (**b**) photo [32].

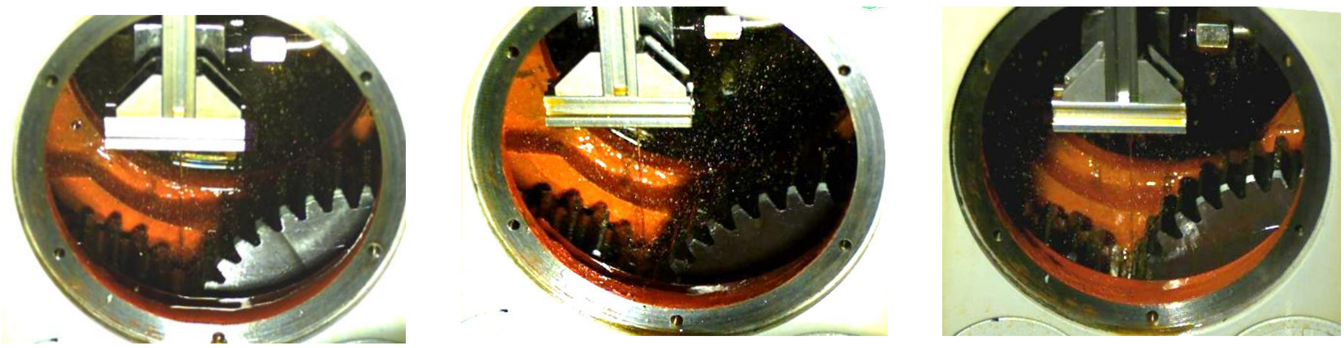

(**a**) (**b**) (**c**)

Figure 17. Oil injection was photographed by a high-speed camera for different groups in Table 2: (**a**) Group 1; (**b**) Group 2; (**c**) Group 3.

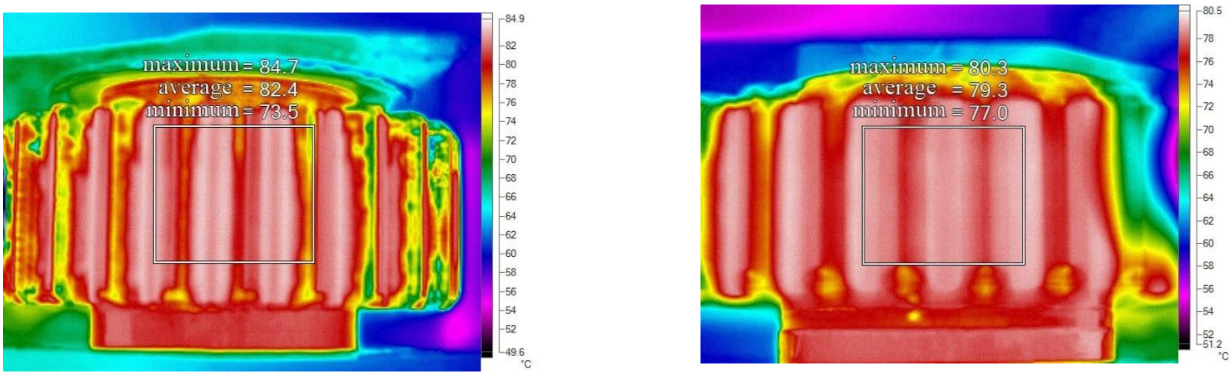

(**a**) (**b**)

Figure 18. Thermography using a thermal infrared imager for Group 2 in Table 2: (**a**) Pinion; (**b**) Gear [32].

Additionally, the experimental tooth surface temperatures are compared with the numerical transient temperatures corresponding to the theoretical impact depths (see Table 5). Along with the increase of the theoretical impingement depth value there is a decrease in the extreme temperature. When the depth reaches 1.1768 mm, the extreme temperature drops to 77.1 °C (experimental) and 69.737 °C (numerical), respectively. The relative errors of extreme temperatures are 9.22%, 10.02%, and 9.21%. This indicates that this method will effectively predict and disclose the temperature field characteristics of the tooth surface. Meanwhile, it also reveals that theoretical impingement depth is an effective measure for evaluating the lubrication and cooling performance.

Table 5. Temperatures corresponding to the theoretical impingement depths.

Group	Impingement Depth of Pinion (mm)	Experimental Maximum Pinion Temperature (°C)	Numerical Maximum Pinion Temperature (°C)
1	0.92198	81.4	73.892
2	1.1768	77.1	69.373
3	0	84.7	76.896

As shown, along with the theoretical impingement depth increasing, the experimental and numerical temperatures reduce, which means better lubrication performance and cooling characteristics are obtained. It is indicated that the numerical method is an effective tool to predict the gear temperature, and the impact depth model can be used to evaluate the oil jet lubrication. It is also evident that the impact depth model can be adopted as an effective tool to estimate lubrication and cooling performance. Lubrication and cooling performance is positively related to the impact depth. Following Wang et al. [41], some suggestions for nozzle layouts for spur gears design can be concluded:

(a) For a gear ratio of 1:1, the deviation distance L and oil injection angle β are recommended to be zero. The impact depth increases with an increase in the ratio of the oil jet velocity to the pitch-line velocity, but the speed at which the impact depth changes decreases gradually.

(b) For a gear ratio larger than 1:1, if the deviation distance L and oil injection angle β are equal to zero, the impact depth of the pinion gradually decreases to zero. Due to the unbiased and inclined nozzle, as the gear ratio increases to a certain value, the impact of the lubricating oil on the tooth of the gear begins to be blocked by its previous tooth. In this case, the lubricating oil jet is completely covered by the gear, and the pinion cannot be sprayed by the lubricating oil. Hence, the impact depth of the pinion decreases to zero. Therefore, to ensure the impact depth of the pinion, the deviation distance L and oil injection angle β of the nozzle towards the pinion should be increased with an appropriate increase in the gear ratio, as depicted in Group 3.

However, it should be pointed out that this paper mainly presents a heat-flow coupled analysis method to predict the transient temperature characteristics of spur gears under different nozzle layouts. The desired quantified formulas for the gear design for nozzle layouts cannot be obtained. Firstly, the definite quantified formulas regarding the optimal nozzle location cannot be elucidated because of the small number of included trials in this paper. Secondly, the nozzle layouts are related to many factors, such as the ratio of oil jet velocity to pitch-line velocity and gear ratio, especially for high-speed conditions where the oil jet flow is influenced by the high-speed air swirl flow. Lastly, the nozzle is limited by the space and shape of the gearbox casing. Therefore, the heat-flow coupled analysis method proposed in this paper is limited to this specific gear design.

5. Conclusions

This paper mainly introduces a heat-flow-coupled analysis method to predict the transient temperature characteristics of spur gears under jet lubrication with different nozzle layouts. Some conclusions are as follows:

(1) The transient temperature for spur gears is modeled based on the mixed EHL model and load contact method, and the differences indicate that the impingement depth is closely related to the nozzle layouts. Specifically, the oil jet height H, deviation distance L, and oil injection angle β have enormous influences on the temperature distribution. Furthermore, it reveals that the greater the impact depth, the lower the transient temperature, and the better the lubrication performance.

(2) When the oil nozzle approaches the side of the pinion (deviation distance $L > 0$, oil injection angle $\beta > 0$, e.g., Group 2 in Table 4), the maximum temperature on the gear tooth is lower, which means better lubrication performance. The numerical method can simulate the temperature distribution characteristics of a spur gear pair and provide some recommendations for the design and installation of the nozzle.

(3) Comparisons of the maximum temperature on the gear tooth with the corresponding impingement depth and experimental results indicate that the numerical method on the transient temperature field is accurate and reliable.

Although the EHL method exploited in this paper is outmoded, it has been proven to be valid and reliable. In future work, the latest thermal EHL method integrating with the toughness model based on an ultra-depth three-dimensional microscope will be introduced for further validation of the numerical investigation method and predicting the temperature distribution with different nozzle layouts.

Author Contributions: Conceptualization, D.Y.; methodology, D.Y.; software, D.Y.; validation, X.Z.; formal analysis, X.Z.; investigation, H.L.; resources, J.Z.; data curation, X.Z.; writing—original draft preparation, X.Z.; writing—review and editing, X.Z.; visualization, X.Z.; supervision, Y.D.; project administration, Y.D.; funding acquisition, Y.D. All authors have read and agreed to the published version of the manuscript.

Funding: This research was funded by the National Defense Preliminary Research Project of China, grant number KY-44-2018-0219, and the General Program of Science and technology on Helicopter Transmission Laboratory, grant number HTL-A-22G10.

Data Availability Statement: All data are contained within the article.

Acknowledgments: We would like to express our thanks to the editors of Lubricants and the anonymous reviewers for their work in processing this article.

Conflicts of Interest: The authors declare no conflict of interest.

References

1. Savolainen, M.; Lehtovaara, A. An experimental investigation of scuffing initiation due to axial displacement in a rolling/sliding contact. *Tribol. Int.* **2018**, *119*, 688–697. [CrossRef]
2. Castro, J.; Seabra, J. Influence of mass temperature on gear scuffing. *Tribol. Int.* **2018**, *119*, 27–37. [CrossRef]

3. Massini, D.; Fondelli, T.; Facchini, B.; Tarchi, L.; Leonardi, F. Experimental investigation on power losses due to oil jet lubrication in high speed gearing systems. In Proceedings of the ASME turbo expo 2017: Turbomachinery Technical Conference and Exposition, Charlotte, NC, USA, 27–29 June 2017. Paper No. GT2017-64703. [CrossRef]
4. Wang, Y.; Niu, W.; Wei, S.; Song, G. Influence of spin flow on lubricating oil jet-design method of oil spray parameters to high speed spur gears. *Tribol. Int.* **2015**, *92*, 290–300. [CrossRef]
5. Wang, Y.; Song, G.; Niu, W.; Chen, Y. Optimized design of spray parameters of oil jet lubricated spur gears. *Tribol. Int.* **2018**, *120*, 149–158. [CrossRef]
6. Wang, Y.; Song, G.; Niu, W.; Chen, Y. Influence of oil injection methods on the lubrication process of high-speed spur gears. *Tribol. Int.* **2018**, *121*, 180–189. [CrossRef]
7. Dowson, D.; Higginson, G.R. A numerical solution to the elasto-hydrodynamic problem. *J. Mech. Eng. Sci.* **1959**, *1*, 6–15. [CrossRef]
8. Yang, P.; Wen, S. A generalized reynolds equation for non-Newtonian thermal elastohydrodynamic lubrication. *J. Tribol.* **1990**, *112*, 631–636. [CrossRef]
9. Akbarzadeh, S.; Khonsari, M.M. Performance of spur gears considering surface roughness and shear thinning lubricant. *J. Tribol.* **2008**, *130*, 021503. [CrossRef]
10. Majumdar, A.; Tien, C.L. Fractal characterization and simulation of rough surfaces. *Wear* **1990**, *136*, 313–327. [CrossRef]
11. Castro, J.; Seabra, J. Global and local analysis of gear scuffing tests using a mixed film lubrication model. *Tribol. Int.* **2008**, *41*, 244–255. [CrossRef]
12. Bobach, L.; Beilicke, R.; Bartel, D.; Deters, L. Thermal elastohydrodynamic simulation of involute spur gears incorporating mixed friction. *Tribol. Int.* **2012**, *48*, 191–206. [CrossRef]
13. Wei, J.; Zhang, A.; Gao, P. A study of spur gear pitting under EHL conditions: Theoretical analysis and experiments. *Tribol. Int.* **2016**, *94*, 146–154. [CrossRef]
14. Ebner, M.; Yilmaz, M.; Lohner, T.; Michaelis, K.; Höhn, B.R.; Stahl, K. On the effect of starved lubrication on elastohydrodynamic (EHL) line contacts. *Tribol. Int.* **2018**, *118*, 515–523. [CrossRef]
15. Venner, C.H. Multilevel Solution of the EHL Line and Point Contact Problems. Ph.D. Thesis, University of Twente, Enschede, The Netherlands, 1991.
16. Fatourehchi, E.; Shahmohamadi, H.; Mohammadpour, M.; Rahmani, R.; Theodossiades, S.; Rahnejat, H. Thermal analysis of an oil jet-dry sump transmission gear under mixed-elastohydrodynamic conditions. *J. Tribol.* **2018**, *140*, 051502. [CrossRef]
17. Fatourehchi, E.; Mohammadpour, M.; Theodossiades, S.; Rahnejat, H. Transient thermal analysis of mixed-elastohydrodynamic contact of high performance transmission in a dry sump environment. *Proc. Inst. Mech. Eng. Part J J. Eng. Tribol.* **2019**, *233*, 326–338. [CrossRef]
18. Rajendhran, N.; Palanisamy, S.; Shyma, A.P.; Venkatachalam, R. Enhancing the thermophysical and tribological performance of gear oil using Ni-promoted ultrathin MoS2 nanocomposites. *Tribol. Int.* **2018**, *124*, 156–168. [CrossRef]
19. Patir, N.; Cheng, H.S. Prediction of the bulk temperature in spur gears based on finite element temperatureanalysis. *ASLE. Trans.* **1979**, *22*, 25–36. [CrossRef]
20. Handschuh, R.F.; Kicher, T.P. A method for thermal analysis of spiral bevel gears. *J. Mech. Des. Trans. ASME* **1996**, *118*, 580–585. [CrossRef]
21. Shi, Y.; Yao, Y.P.; Fei, J.Y. Analysis of bulk temperature field and flash temperature for locomotive traction gear. *Appl. Therm. Eng.* **2016**, *99*, 528–536. [CrossRef]
22. Li, W.; Tian, J.Y. Unsteady-state temperature field and sensitivity analysis of gear transmission. *Tribol. Int.* **2017**, *116*, 229–243. [CrossRef]
23. Wang, Y.; Tang, W.; Chen, Y.; Wang, T.; Li, G.; Ball, A.D. Investigation into the meshing friction heat generation and transient thermal characteristics of spiral bevel gears. *Appl. Therm. Eng.* **2017**, *119*, 245–253. [CrossRef]
24. Zhang, J.G.; Liu, S.J.; Fang, T. Determination of surface temperature rise with the coupled thermo-elasto-hydrodynamic analysis of spiral bevel gears. *Appl. Therm. Eng.* **2017**, *124*, 494–503. [CrossRef]
25. Akin, L.S.; Townsend, D.P. Into mesh lubrication of spur gears with arbitrary offset oil jet. part 1: For jet velocity less than or equal to gear velocity. *ASME J. Mech. Trans. Autom.* **1983**, *105*, 713–718. [CrossRef]
26. Akin, L.S.; Townsend, D.P. Into mesh lubrication of spur gears with arbitrary offset oil jet. part 2: For jet velocities equal to or greater than gear velocity. *ASME J. Mech. Trans. Autom.* **1983**, *105*, 719–724. [CrossRef]
27. Akin, L.S.; Townsend, D.P. Lubricant jet flow phenomena in spur and helical gears with modified center distances and/or addendums-for out-of-mesh conditions. *ASME J. Mech. Trans. Autom.* **1985**, *107*, 24–30. [CrossRef]
28. Huang, C.H.; Huang, Y.R. An optimum design problem in estimating the shape of perforated pins and splitters in a plate-pin-fin heat sink. *Int. J. Therm. Sci.* **2021**, *170*, 107096. [CrossRef]
29. Dai, Y.; Xu, L.; Zhu, X.; Ouyang, B. Application of an unstructured overset method for predicting the gear windage power losses. *Eng. Appl. Comp. Fluid* **2021**, *15*, 130–141. [CrossRef]
30. Jiang, L.; Lyu, Y.; Zhu, P. Numerical investigation of conjugate heat transfer on a rotating disk under round liquid jet impingement. *Int. J. Therm. Sci.* **2021**, *170*, 107097. [CrossRef]
31. Dai, Y.; Wu, W.; Zhou, H.B.; Zhang, J.; Ma, F.Y. Numerical simulation and optimization of oil jet lubrication for rotorcraft meshing gears. *Int. J. Simul. Model* **2018**, *17*, 318–326. [CrossRef]

32. Dai, Y.; Ma, F.; Zhu, X.; Su, Q.; Hu, X. Evaluation and optimization of the oil jet lubrication performance for orthogonal face gear drive: Modelling, simulation and experimental validation. *Energies* **2019**, *12*, 1935. [CrossRef]
33. Zhu, X.; Dai, Y.; Ma, F.; Ouyang, B. Mathematical modeling and numerical simulation for determining an optimized oil jet layout for spiral bevel gear. *Proc. Inst. Mech. Eng. Part J J. Eng. Tribol.* **2021**, *235*, 611–628. [CrossRef]
34. Ouyang, B.; Ma, F.; Dai, Y.; Zhang, Y. Numerical analysis on heat-flow-coupled temperature field for orthogonal face gears with oil–jet lubrication. *Eng. Appl. Comp. Fluid* **2021**, *15*, 762–780. [CrossRef]
35. Dudley, D.W. *Dudley's Gear Handbook*; Tata McGraw-Hill Education: New York, NY, USA, 1991.
36. Bair, S.; Winer, W.O. A rheological model for elastohydrodynamic contacts based on primary laboratory data. *J. Lubr. Technol.* **1979**, *101*, 258–264. [CrossRef]
37. Zhu, D.; Hu, Y.Z. A computer program package for the prediction of EHL and mixed lubrication characteristics, friction, subsurface stresses and flash temperatures based on measured 3-D surface roughness. *Tribol. Trans.* **2001**, *44*, 383–390. [CrossRef]
38. Hu, Y.Z.; Zhu, D. A full numerical solution to the mixed lubrication in point contacts. *J. Tribol.* **2000**, *122*, 1–9. [CrossRef]
39. Gan, L.; Xiao, K.; Wang, J.; Pu, W.; Cao, W. A numerical method to investigate the temperature behavior of spiral bevel gears under mixed lubrication condition. *Appl. Therm. Eng.* **2019**, *147*, 866–875. [CrossRef]
40. Lienhard, J.H.; Catton, I. Heat transfer across a two-fluid-layer region. *ASME J. Heat Transfer.* **1986**, *108*, 198–205. [CrossRef]
41. Wang, X.; Liu, S.J.; Hu, Y. Analysis of influence factor of oil jet lubrication impingement depth of aviation spur gear. *J. Mech. Transm.* **2017**, *41*, 23–29. (In Chinese) [CrossRef]